metals

MDPI

Article

A Study on the Effect of Ladle Structures and Stirrer Positions on the Internal Flow Field in the Hot Metal Desulfurization Process

Lifei Wang [1,2,3], Qingchun Yu [1,2,3,*], Shubiao Yin [1,*], Guozhi Wang [1,2,3] and Songlai Zhang [1,2,3]

[1] Faculty of Metallurgical and Energy Engineering, Kunming University of Science and Technology, Kunming 650093, China; wanglifei626@163.com (L.W.); 17864889995@163.com (G.W.); zslkmust@163.com (S.Z.)
[2] National Engineering Research Center of Vacuum Metallurgy, Kunming University of Science and Technology, Kunming 650093, China
[3] Key Laboratory for Nonferrous Vacuum Metallurgy of Yunnan Province, Kunming University of Science and Technology, Kunming 650093, China
* Correspondence: yqcy@163.com (Q.Y.); yinshubiao@kust.edu.cn (S.Y.)

Abstract: The geometry of the ladle bottom and the position of stirring paddles during hot metal stirring significantly influence hydrodynamic characteristics, thereby affecting desulfurization efficiency. Water model experiments and hydrodynamic simulations were conducted to investigate the effects of ladle structures and stirrer positions on the flow field and mixing characteristics in hot metal desulfurization. The results indicate that ladles with a spherical-bottom structure effectively reduced the "dead zone" volume in the hot metal flow. In the water model tests, the mixing time for the spherical-bottom ladle was reduced by 22.5% and 20% at different stirring paddle speeds compared to the flat-bottom ladle, facilitating the better dispersion of the desulfurization agents. The hot metal flow velocities in all directions were also superior in spherical-bottom ladles. Under identical conditions, eccentric stirring generated shallower and broader vortices, with the vortex center offset from the stirring shaft axis, thereby minimizing the risk of "air entrainment" associated with high-speed central stirring. During eccentric stirring, the flow-field distribution was uneven, and the polarization of the stirrer was observed in the water model, whereas central stirring revealed a more uniform and stable flow field, reducing the risk of paddle wear and ladle wall erosion. Central stirring exhibits distinct advantages in the desulfurization process, whereas eccentric stirring is exclusively applicable to metallurgical modes requiring a rapid enhancement of bottom flow and localized rapid dispersion of desulfurizing agents.

Keywords: desulfurization; ladle; velocity distribution; mixing time

Academic Editor: Hong Yong Sohn

Received: 13 December 2024
Revised: 14 January 2025
Accepted: 16 January 2025
Published: 18 January 2025

Citation: Wang, L.; Yu, Q.; Yin, S.; Wang, G.; Zhang, S. A Study on the Effect of Ladle Structures and Stirrer Positions on the Internal Flow Field in the Hot Metal Desulfurization Process. *Metals* **2025**, *15*, 90. https://doi.org/10.3390/met15010090

1. Introduction

Elemental sulfur, a harmful impurity in steel, forms iron sulfide, which induces brittleness during heat treatment, weakens the bonding between grains, and reduces both the mechanical properties and productivity of the steel [1,2]. The sulfur content in steel must be limited to <60 ppm to enable enhanced treatment during the secondary refining stage, improving deoxidation and cleanliness. Certain special steel grades, such as low-carbon (LC) steel, ultra-low-carbon (ULC) steel, and electrical steel, also have sulfur limits, with sulfur content restricted to <120 ppm [3]. Currently, various hot metal desulfurization technologies are employed, with the Kanbara reactor (KR) desulfurization [4] and powder injection desulfurization [5] being the primary methods [6–9]. Compared to the blowing method, the

KR method offers significant advantages in deep desulfurization, desulfurization stability, equipment simplicity, and high operability, making it an essential process in the production of high-quality steel. However, the turbulence generated during the high-speed stirring process in the KR method often impacts the stirring paddles and furnace lining, leading to the erosion of the furnace lining and wear of the stirring paddles, which ultimately reduces the service life of the reactor [10]. Therefore, when evaluating the internal flow field of the hot metal stirring process, it is essential to consider the service life of both the reactor and stirring equipment comprehensively.

In recent years, the primary research methods for mechanical mixing have included field observation experiments [11], water model experiments, and numerical simulations. Field observation experiments are constrained by various complexity factors, making it challenging to precisely control experimental conditions. For instance, full-scale production experiments are limited by high costs, extreme operational environments, and the inability to directly observe the molten steel flow field. As a result, researchers must rely on indirect measurements or numerical simulations for analysis, inevitably introducing a degree of uncertainty into the results. In contrast, water model experiments can be conducted in a controlled environment, offering lower costs and higher reproducibility. Numerical simulations, on the other hand, provide a theoretical foundation for optimizing the desulfurization process by precisely calculating the flow field and temperature distribution, allowing for the analysis of internal flow-field characteristics without risk. Relevant water modeling studies have shown that the region of strongest mass transfer occurs between the forced vortex radius in the ladle and the end of the stirring paddle. The movement trajectory of suspended particles (desulfurizing agent particles) follows a cyclical pattern: vortex entrainment, dispersion, upward floating to the vortex, and re-entrainment [12]. Improving the design of the stirring paddle can effectively increase the depth of the stirring vortex and enhance the dispersion of desulfurizing particles [13], improving the mixing efficiency in the area beneath the impeller [14]. The desulfurization kinetics of calcium oxide as a desulfurizing agent indicate that the desulfurization reaction at the CaO–hot metal interfacial flow is relatively fast, with the diffusion step being the rate-limiting stage of the desulfurization process [15]. Consequently, the mixing time of desulfurizing particles within the hot metal ladle is a crucial factor influencing the desulfurization efficiency. Increasing the paddle speed and deepening the paddle immersion depth can effectively shorten the mixing time [16]. Xu A. J. et al. [17] found that the order of significance for the factors affecting mixing time was as follows: stirring speed > paddle depth > amount of iron > paddle position. Among these, stirring speed had the most significant impact on mixing time, and eccentric stirring was not recommended. The shortest mixing time was observed when the stirring speed was 125 rpm, and the paddle immersion depth was 280 mm. With the continuous advancement in flow-field technology for stirred reactors, methods to study the interaction between fluid and stirrer have evolved, including the impeller boundary condition (IBC) [18], momentum source (MS) model [19], inner–outer (IO) [20], multiple reference frame (MRF) [21], and sliding mesh (SM) methods [22]. Currently, the MRF and SM methods are widely applied in stirred tank simulations due to their high accuracy. Numerical simulations of the stirrer structure's effect on the KR hot metal desulfurization process have yielded results consistent with water model studies. The staggered blade configuration improves the desulfurization efficiency of the KR process [23], while modifications to the impeller design [24] and desulfurizer particle addition technology can further enhance desulfurization efficiency [25]. Additionally, higher impeller speeds (80–120 rpm) and elevated temperatures (1573–1673 K) are also effective methods [26]. The simulation of desulfurizer particle movement in mechanically stirred hot metal shows that a properly set eccentricity leads to better mixing [24], and desulfurization efficiency improves when the impeller

eccentricity is 100 mm [27], which contrasts with the findings of Xu A. J. et al. [17] in their water model study.

Previous studies on the desulfurization of KR hot metal have primarily focused on the impact of stirrer design on the internal flow field, with limited attention given to the influence of ladle structure on the desulfurization process. Additionally, the exploration of eccentric stirring has been met with some controversy in the existing literature [17,24,27], and most studies concentrate solely on desulfurization efficiency, without offering a comprehensive assessment of equipment wear during the stirring process. As a result, these studies often overlook the balance between desulfurization efficiency and equipment performance. Theoretically, a spherical bottom has a smooth surface, which facilitates the smooth flow of fluids and enhances mixing efficiency. The design of the spherical bottom is functionally similar to the sloped bottom in metal production, effectively promoting fluid mixing and power transfer. Spherical-bottom ladles offer clear advantages over other ladle types. Relevant studies have shown that spherical-bottom stirring tanks require approximately 10 to 20 percent less power than flat-bottom stirring tanks [28]. Since the density of desulfurizing agent particles is typically lower than that of hot metal, the effective dispersion of these particles is crucial. One key factor is the rapid entry of desulfurizer particles into the molten metal, ensuring their uniform distribution during the reaction. Considering the dependency of flow phenomena on bottom geometry, the mixing times and associated parameters for conventional flat-bottom ladles may not be applicable when extrapolated to spherical-bottom ladles. Compared to conventional central desulfurization stirring, eccentric stirring increases the contact between hot metal and desulfurizer by enhancing flow rate and shear forces, thereby accelerating the desulfurization reaction. However, the asymmetric structure of eccentric stirring may result in an uneven desulfurization process and could lead to operational instability. Therefore, studying the flow-field characteristics and the effects of eccentric desulfurization stirring in spherical-bottom ladles is of significant theoretical and practical importance for achieving a high-quality, uniform, and stable desulfurization process.

This study focuses on the investigation of fluid flow through mathematical simulations and water modeling. The VOF model in ANSYS Fluent 2022 R2 software was employed to track the position of and changes in the iron–air interface, while the MRF model was utilized to simulate fluid dynamics between the rotating and stationary regions. Additionally, a quasi-k–ε turbulence model was coupled to characterize the turbulence behavior during the mixing process. The effects of spherical-bottom and flat-bottom ladle geometries on fluid flow and mixing behavior in mechanically stirred ladles at varying rotational speeds were evaluated. Furthermore, the differences in the external vortices and internal flow fields generated by central and eccentric desulfurization stirring were analyzed to systematically assess the advantages and disadvantages of eccentric versus central desulfurization. The primary motivation for this work is to provide a foundation for industrial applications.

2. Materials and Methods

2.1. Water Model Experiment

Due to the large volume of industrial steel ladles, as shown in Figure 1a,b, a water model stirring system made of plexiglass was constructed in this experiment based on a 210-ton industrial steel ladle according to the principle of geometric similarity. The actual production process was simulated by observing the water flow. The scale ratio between the water model stirring system and the actual 210-ton KR desulfurization steel ladle was 1:10. An electric digital stirrer JJ-1A100W (manufactured by Xicheng Xinrui Instrument Factory, Jintan District, Changzhou, Jiangsu, China) with a maximum rotational speed of 3000 rpm was used in the water model stirring system. The immersion depth of the stirring paddle

was 217.5 mm, and the stirring speed was adjustable at 120, 160, and 200 r/min. The liquid depth was set at 300 mm. Experimental studies were conducted on both flat-bottom and spherical-bottom ladles, examining the desulfurization effect at the center of the flat-bottom ladle and at a point that was offset 30 mm from the axis. The detailed dimensions of the ladle and impeller are provided in Table 1. A high-speed camera was used to capture the stirring state of the liquid surface, recording vortex shape and depth changes and investigating the influence of stirring process parameters on the KR's desulfurization effect.

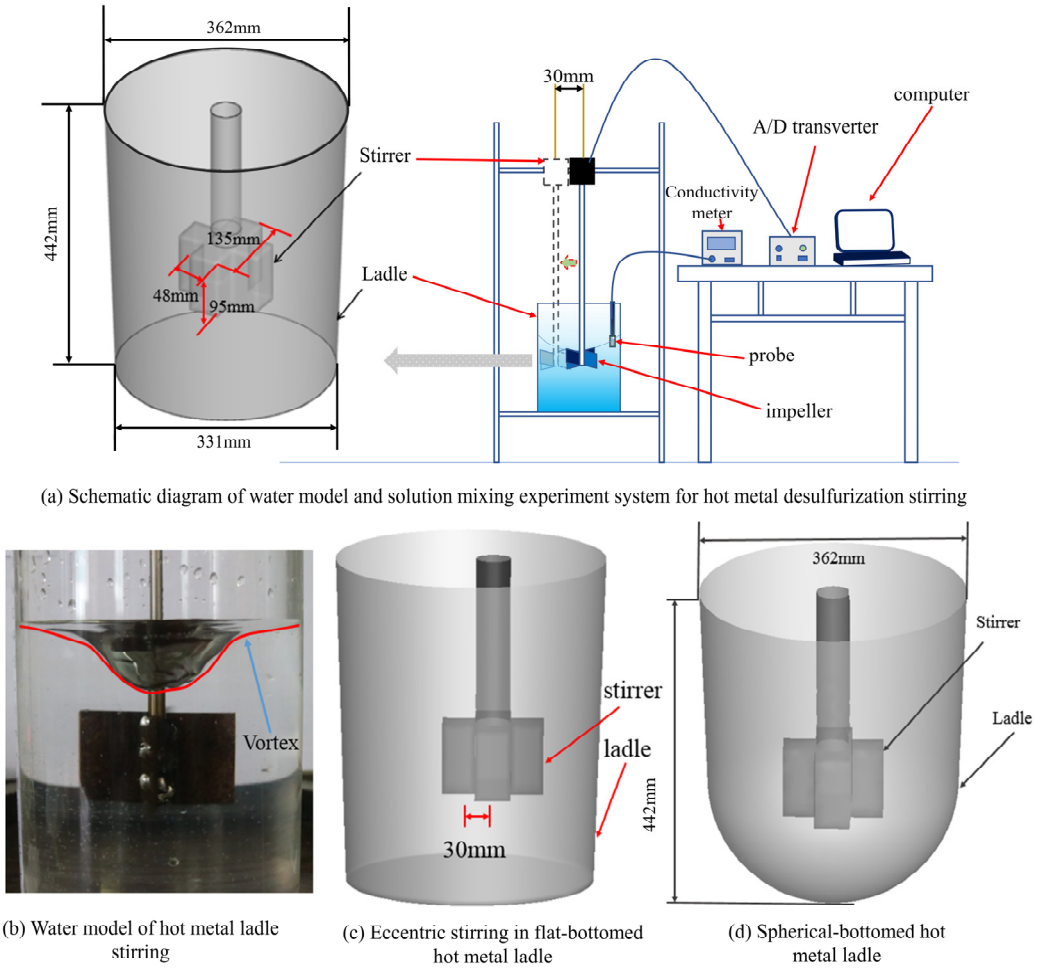

(a) Schematic diagram of water model and solution mixing experiment system for hot metal desulfurization stirring

(b) Water model of hot metal ladle stirring

(c) Eccentric stirring in flat-bottomed hot metal ladle

(d) Spherical-bottomed hot metal ladle

Figure 1. Water model and experimental system for solution mixing during iron desulfurization stirring, along with the geometric model of the iron ladle.

Table 1. Dimensions of the ladle and stirring impeller.

Parameters	210-Ton Capacity Ladle	Water Model (1:10)
Top ladle diameter (mm)	3620	362
Bottom ladle diameter (mm)	3360	331
Ladle height (mm)	4420	442
Surface level (mm)	3370 (210 t)	336
diameter of impeller (mm)	1350	135
Impeller height (mm)	950	95
Impeller blade thickness (mm)	480	48

To ensure the principle of dynamic similarity and make the experimental results of the water model reflective of actual conditions, it is necessary to correlate the experimental parameters in the water model with the actual process parameters. According to the

similarity principle, the Froude numbers Fr of the water model and the prototype should be equal [29], as shown in Equation (1):

$$\frac{gL_w}{\left(\frac{N_w r_w^3}{Kd_w^5\rho_w}\right)^{\frac{2}{3}}} = \frac{gL_l}{\left(\frac{N_l r_l^3}{Kd_l^5\rho_l}\right)^{\frac{2}{3}}} \quad (1)$$

where the subscripts w and l represent the water model and the actual steel ladle, respectively; K is the power factor; N is the theoretical power (kW); d and r are the diameter and radius of the stirring impeller, respectively, in meters m; ρ is the density; and g is the gravitational acceleration, in meters per second squared (m s^{-2}). Due to geometric similarity, $\frac{r_w}{r_l} = \frac{d_w}{d_l} = \frac{L_w}{L_l} = \frac{1}{10}$. The theoretical power calculation formula is as follows:

$$N = \frac{K\rho n^3 d^5}{1000} \quad (2)$$

Thus, we have

$$N_w = 3.15N_l, n_w = 3.15n_l \quad (3)$$

where n represents the rotational speed, with the unit rpm. This indicates that the speed ratio between the KR molten iron stirring desulfurization model and actual production is 1:3.15. The parameter utilized in this study is presented in Table 2.

Table 2. Parameters used in the water model.

Parameters	210-Ton Capacity Ladle	Water Model (1:10)
Rotation speed (rpm)	38, 50.7, 63.5	120, 160, 200
Liquid density (kg m^{-3})	7020	1000
Impeller immersion depth (mm)	1575, 2175	157.5, 217.5
Liquid viscosity (Pa·s)	0.0064	0.001

2.2. Solution Mixing Experiment

Mixing time is a value that renders useful information, and this parameter is often used as an indicator of stirring effectiveness. The conductivity method is widely employed in investigations on the influential factors of determined mixing time [7]. This method is based on the principle of monitoring the change in electrical conductivity within the mixed liquid. The conductivity was measured as a function of time by using conductivity electrodes. In this experiment, a conductivity probe supplied with a digital conductivity meter DDSJ-308A (manufactured by Shanghai INESA Scientific Instrument Co., Ltd., Shanghai, China) was employed to record changes in the local ion concentration of a pulse tracer (KCl). To ensure that the measurements accurately reflect the overall mixing behavior within the water model, and considering the difficulty of securing the conductivity probe at the bottom of the spherical-bottom model, the probe was installed at a depth of 395 mm near the sidewall of the water model. The mixing process was regarded as complete when the electrical conductivity within the mixed liquid did not change with time. This point was reached when the change in conductivity was within a 5 pct deviation of the well-mixed/homogeneous value [30]. Experimental data were subsequently analyzed, and a plot of conductivity vs. time was generated. Corresponding mixing times were estimated. After adding the tracer, significant oscillations in conductivity were observed, which essentially resulted from the periodic fluctuations in the amount of tracer passing through the probe tip [31,32].

3. Mathematical Simulation

In this study, ANSYS FLUENT software was employed to simulate the stirring process during iron desulfurization. In the model, the X and Y axes were centered at the origin of the ladle's horizontal cross-section, while the Z axis was defined with the origin set 3000 mm downward from the top of the ladle. The geometric model for hot metal desulfurization is shown in Figure 1a,c,d. The simulation modeled the flow of hot metal driven with a stirrer to enhance the desulfurization efficiency. The model assumed that the physical properties of hot metal remained constant, disregarding the effects of temperature variations, chemical reactions, and the slag layer on the hot metal surface. A volume of fluid (VOF) model was employed to capture the dynamic behavior of the gas–liquid interface, while a standard k-ε turbulence model was utilized to characterize the turbulence during the stirring process. The agitator region was modeled using a multiple reference frame (MRF) approach, in which the internal region containing the agitator was defined as a rotating reference frame, while the external region was defined as a stationary reference frame. Inertial forces, such as Coriolis forces, were incorporated into the momentum equations within the rotating reference frame, enabling an accurate description of the flow behavior of rotating fluids through the decomposition of absolute and relative velocities. The model considered hot metal and air as continuous phases and incorporated mathematical equations for mass conservation, momentum conservation, turbulent kinetic energy, and turbulent dissipation rate to describe the flow dynamics within the continuous phase. The volume of fluid (VOF) model was employed to track the position and evolution of the hot metal–air interface, while the multiple reference frame (MRF) model ensured the accurate coupling of hydrodynamic interactions between the rotating and stationary regions.

3.1. Assumptions and Premises

The following assumptions were made to simplify the numerical model for iron desulfurization stirring:

1. The interface between the iron and gas phases (with the gas phase referring specifically to air) is well defined, making it suitable for the volume of fluid (VOF) model, which effectively captures and tracks the gas–liquid interface without considering the miscibility or diffusion processes between the gas and liquid phases.
2. The turbulence during the mixing process was assumed to be homogeneous, with the turbulent kinetic energy k and dissipation rate ϵ accurately described by the standard k-ϵ model, whose empirical constants were validated for the present working conditions.
3. Assuming that the sum of the volume fractions of the fluids in each computational cell equaled 1 and considering both the ferrous and gaseous phases as incompressible fluids, the continuity equation was fulfilled.

3.2. Mesh Generation

The geometric model of iron mixing desulfurization, as illustrated in Figure 1a–c, was meshed using the ICEM module in ANSYS. To ensure computational accuracy, the mesh was divided into structured and unstructured grids. As illustrated in Figure 2a,b, the irregular internal structure of the mixer necessitated the use of an unstructured mesh for the internal region, while the external region, being more regular, was meshed using a structured grid, as shown in Figure 2c. The internal and external meshes were then coupled to ensure seamless data transfer between the two regions. The vertical and horizontal cross-sectional meshes of the flat-bottom iron water geometric model are depicted in Figure 2d. Grid adjustments for axial and eccentric mixing studies are shown in Figure 2e,f. To evaluate grid independence, four grid densities were tested: 12,960 cells, 29,160 cells,

69,120 cells, and 135,000 cells. Simulations were conducted for a flat-bottom iron ladle at a rotational speed of 160 rpm. The results indicate that starting from resolution 3, the predictions became grid-independent. When the grid density increased to 69,120 cells, the calculations converged, with relative errors of key variables remaining below 1%. For the ladle case, the simulation results of the vertical and horizontal sections demonstrate that the differences in key parameters between 69,120 and 135,000 cells were less than 0.5%, verifying that the adopted grid density was sufficient to meet the required calculation accuracy. The adopted combination of structured and unstructured meshing ensured both geometric adaptability and computational efficiency, achieving accuracy and stability in the simulation results. The scientific validity and rationality of the meshing scheme were verified through grid independence testing, providing a reliable foundation for subsequent numerical simulations.

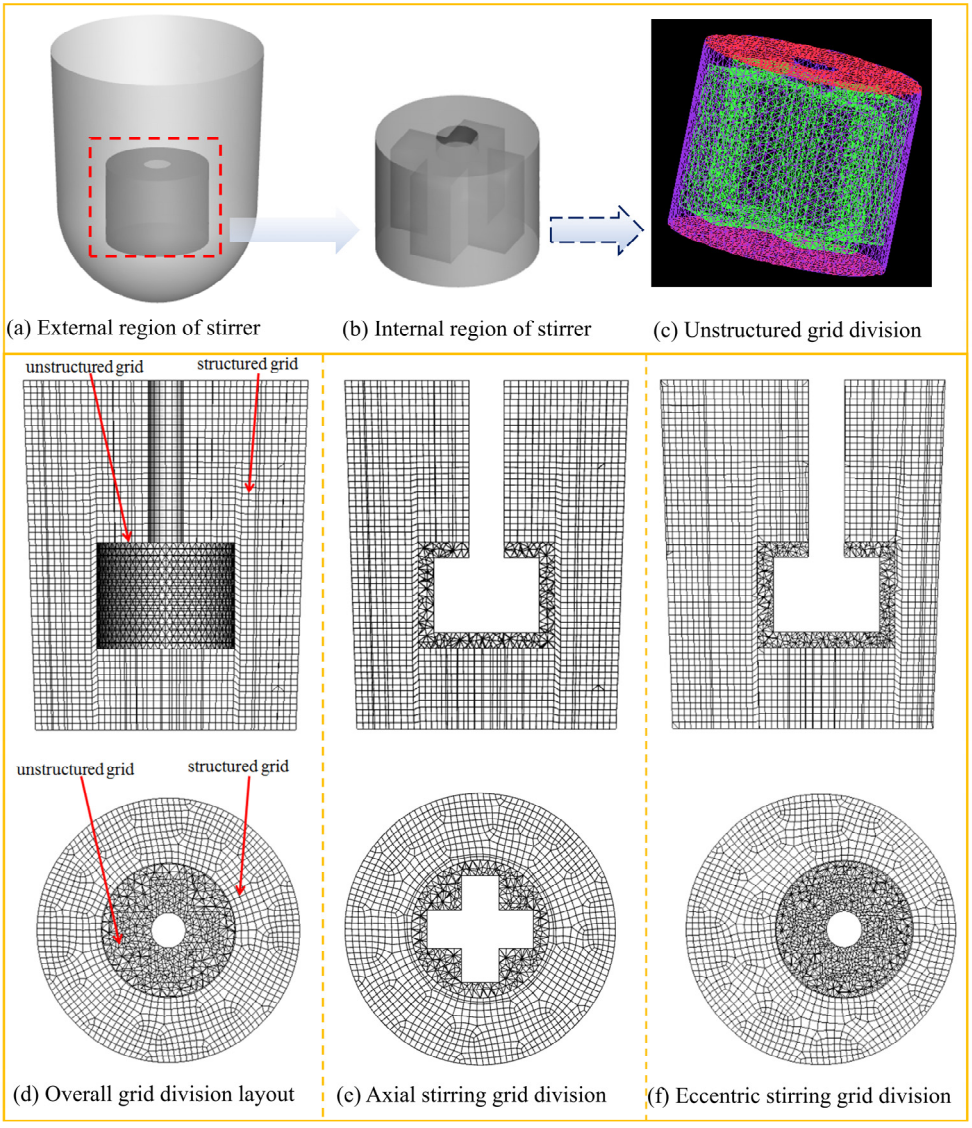

Figure 2. Grid division for iron mixing desulfurization.

3.3. Governing Equations

3.3.1. Multiphase Flow VOF Model

Iron desulfurization stirring requires the simulation of stirring vortices, specifically the numerical modeling of gas–liquid interfaces. The primary approaches for simulating such multiphase flows include the Euler–Euler and Euler–Lagrange methods. Among

these, the volume of fluid (VOF) model within the Euler–Euler framework is well suited for simulating multiphase flows without phase mixing, as it accurately captures and tracks the interfaces between different phases [33]. For the continuous phase, the continuity equation is described as follows:

$$\frac{\partial}{\partial t}(\alpha_q \rho_q) + \nabla \cdot (\alpha_q \rho_q \overline{v}_q) = 0 \tag{4}$$

$$\sum_{q=1}^{m} \alpha_q = 1 \tag{5}$$

where α_q is the volume fraction of the q phase; $\overline{v}_q$ is the velocity of the q phase, m/s; ρ_q is the density of the q phase, kg/m^3; t is the calculation time, s; and m is the total number of the continuous phases. The volume fraction αq of each phase was computed as follows [34]:

$$\frac{\partial(\alpha_q)}{\partial t} + \overline{v}_q \cdot \nabla \alpha_q = 0 \tag{6}$$

Each calculation cell contains liquid and solid phases, in which the sum of the volume fractions of the phases is equal to 1, as shown in Equation (5). The momentum equation is as follows:

$$\frac{\partial}{\partial t}(\rho \overline{v}_q) + \nabla \cdot (\rho \overline{v}_q \overline{v}_q) = -\nabla p + \nabla \left[\mu \left(\nabla \overline{v}_q + \nabla \overline{v}_q^T \right) \right] + \rho g + F \tag{7}$$

$$\rho = \sum_{q=1}^{m} \alpha_q \rho_q \tag{8}$$

$$\mu = \sum_{q=1}^{n} \alpha_q \mu_q \tag{9}$$

where α_q is the volume fraction of the q phase; μ_q is the viscosity of the q phase, kg/(m·s); ρ_q is the density of the q phase, kg/m^3; and F represents the interaction force between each phase [35].

3.3.2. k-ε Turbulence

The standard k-ε model [36] was employed to calculate the turbulent parameters. The turbulent kinetic energy k and turbulent dissipation rate ε were, respectively, calculated as follows:

$$\frac{\partial}{\partial t}(\rho_l \kappa) + \frac{\partial}{\partial x_i}(\rho_l \kappa v_i) = \frac{\partial}{\partial x_j}\left[\left(\mu + \frac{\mu_t}{\sigma_k} \right) \frac{\partial k}{\partial x_j} \right] + G_k - \rho_l \varepsilon \tag{10}$$

$$\frac{\partial}{\partial t}(\rho_l \varepsilon) + \frac{\partial}{\partial x_i}(\rho \varepsilon v_i) = \frac{\partial}{\partial x_j}\left[\left(\mu + \frac{\mu_t}{\sigma_\varepsilon} \right) \frac{\partial \varepsilon}{\partial x_j} \right] + C_{1\varepsilon} \frac{\varepsilon}{k} G_k - C_{2\varepsilon} \rho_l \frac{\varepsilon^2}{k} \tag{11}$$

where ρ_l is the density of hot metal, kg/m^3; x_i and x_j are the coordinates in the i direction and j direction in m, respectively; v_i is the velocity in the i direction, m/s; μ_t is the turbulent viscosity, kg/(m·s); G_k is the generation of turbulence kinetic energy due to the mean velocity gradients, kg/(m·s^3); k and ε are the turbulent kinetic energy and turbulent dissipation rate, respectively; σ_k and σ_ε are the turbulent Prandtl numbers for k and ε, respectively; and $C_{1\varepsilon}$ and $C_{2\varepsilon}$ are constants; the value of constants are $C_{1\varepsilon}$ = 1.44, $C_{2\varepsilon}$ = 1.92, σ_k = 1.0, and σ_ε = 1.3 [36].

3.3.3. MRF Multiple Reference System Modeling

The inner region containing the stirrer, as shown in Figure 2b, is defined as a rotating reference frame, while the outer region is treated as a stationary reference frame. The multiple reference frame (MRF) model is an effective method for simulating fluid flow in rotating

systems. When solving equations in a rotating coordinate system, the fluid acceleration must be accounted for in the momentum equation. This acceleration is calculated using the relationship between absolute and relative velocities, which is expressed as follows:

$$\mathrm{v_r} = \mathrm{v} - (\Omega \times \mathrm{r}) \tag{12}$$

where v represents the absolute velocity, $\mathrm{v_r}$ denotes the relative velocity, Ω is the angular velocity of rotation, and r is the position vector. In the rotating coordinate system, the left-hand side of the momentum equation, expressed in terms of absolute velocity, can be written as follows:

$$\frac{\partial}{\partial t}(\rho v) + \bigtriangledown \cdot (\rho v_r v) + \rho(\Omega \times v) \tag{13}$$

Expressed in terms of relative velocity, it can be written as follows:

$$\frac{\partial}{\partial t}(\rho v_r) + \bigtriangledown \cdot (\rho v_r v) + \rho(2\Omega \times v_r + \Omega \times \Omega \times r) + \rho\frac{\partial \Omega}{\partial t} \times \mathrm{r} \tag{14}$$

where ρ(2Ω × vr) represents the Coriolis force.

4. Results and Discussion

4.1. Validation of Numerical Simulation and Water Model

The appearance of the water models for the different bottom designs is not compared here, as the difference in the swirl patterns at the top of the flat-bottom and spherical-bottom ladles is minimal. However, significant differences were observed between the two bottom designs with respect to the internal flow dynamics of hot metal and water. The water model was validated by measuring the mixing time of desulfurized particles in the hot metal during mixing, using conductivity measurements. Since the flow-field distribution in the flat-bottom iron ladle was more uniform, the influence of other factors was relatively small. Subsequent modeling and experimental studies on eccentric and central iron desulfurization were conducted in the flat-bottom iron ladle.

In the water model experiments, the mixing time was determined by measuring the conductivity, and the results were compared with those from related studies to validate the accuracy of the water model. A deviation in conductivity of less than 5% was considered indicative of complete mixing [30]. The mixing time was defined as the duration from the initial change in conductivity to its eventual stabilization. The experimental setup used for determining mixing time in the water model experiment is shown in Figure 1a.

An appropriate stirring paddle speed was selected to compare the effects of spherical-bottom and flat-bottom ladles on mixing time. Experiments were conducted at stirring speeds of 90 rpm and 120 rpm, and the relationship between conductivity and time was recorded, as shown in Figure 3. Upon the addition of sodium chloride solution, conductivity exhibited a transient increase before stabilizing. At 90 rpm, the mixing times for the spherical-bottom and flat-bottom ladles were 12.7 s and 16.4 s, respectively. At 120 rpm, the mixing times were 8 s and 10 s, respectively, with the spherical-bottom ladle showing reductions of 22.5% and 20%. This indicates that spherical-bottom ladles reduce the mixing time, thereby improving the efficiency of iron desulfurization. Furthermore, increasing the stirring speed from 90 rpm to 120 rpm resulted in a decrease in mixing time, consistent with the thermodynamic and kinetic simulation studies of the KR desulfurization method by Xu An-jun et al. [17]. These results confirm the validity of the water model used in this study and provide valuable guidance for subsequent modeling and experimental work.

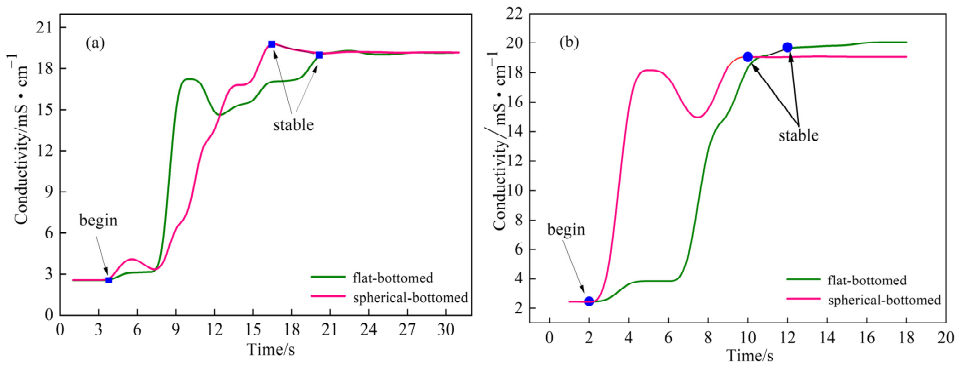

Figure 3. Relationship between conductivity and stirring time: (**a**) stirring speed of 90 rpm; (**b**) stirring speed of 120 rpm.

Figure 4 presents a comparison between the numerical simulation and the water model test under different conditions of central stirring and eccentric stirring. Based on the previously discussed principles of geometric similarity and dynamic similarity, the parameters between the two approaches were highly consistent, enabling mutual verification and ensuring the effectiveness of the comparison. In subsequent analyses, detailed parameter correspondence will not be repeatedly explained, and the dimensions of the water model will primarily guide the discussion. In Figure 4a, the numerical simulation depicts the vortex shape for central desulfurization stirring, with the stirrer immersed to a depth of 157.5 mm and a stirring speed of 120 rpm. The resulting vortex appears as an inverted cone, with both its shape and depth closely aligning with the observations from the water model test, where the stirrer immersion depth was 175.5 mm. Figure 4b illustrates the results of the numerical simulation and the water model test for eccentric desulfurization stirring. In this scenario, the stirrer was submerged to a depth of 217.5 mm, with a stirring speed of 120 rpm. The vortex patterns generated in the numerical simulation exhibit similar characteristics to those observed in the water model test at an identical immersion depth of 217.5 mm, with comparable vortex depths. The maximum vortex depth is located near the center of the stirring tank, though it does not align with the rotational shaft's center. The combined validation of numerical simulation and water model testing demonstrates the reliability and accuracy of the simulation in capturing the stirring behavior during the hot metal desulfurization process, providing robust support for this study.

As shown in Figure 5, the depth of the inverted conical vortex increased as the stirring speed accelerated, with the stirring speed gradually rising from 120 to 200 rpm. Both the numerical simulation and experimental results show that the vortex depth increased with speed, consistent with theoretical predictions. This phenomenon was more pronounced in central desulfurization, indicating that the numerical simulation modeling method can reliably reflect fluid behavior in the actual stirring process. At the same stirring speed, as shown in Figure 6, when the stirring paddle was immersed to a shallower depth of 157.5 mm, a noticeable air entrainment phenomenon was observed in the hot metal. This phenomenon is caused by the introduction of air as the vortex depth reaches a critical threshold under these conditions. This increases the oxygen content in the hot metal, which hinders the desulfurization reaction and may also reduce the overall desulfurization efficiency. In practical production scenarios, such effects can significantly impair the hot metal desulfurization process. Figure 5 presents a comparison of the vortex shapes in eccentric and central desulfurization. At the same immersion depth, the horizontal area at the bottom of the vortex generated by the eccentric mixing process was significantly larger than that produced by central mixing, while its depth was shallower. At the same mixing speed and depth, eccentric desulfurization effectively minimized air entrainment. Additionally, the larger horizontal area of the vortex facilitated the coil

suction and dispersion of the desulfurizing agent, thus enhancing desulfurization efficiency. Moreover, the stirring depth should be controlled within the critical range that produces a strong stirring effect while avoiding the introduction of air bubbles.

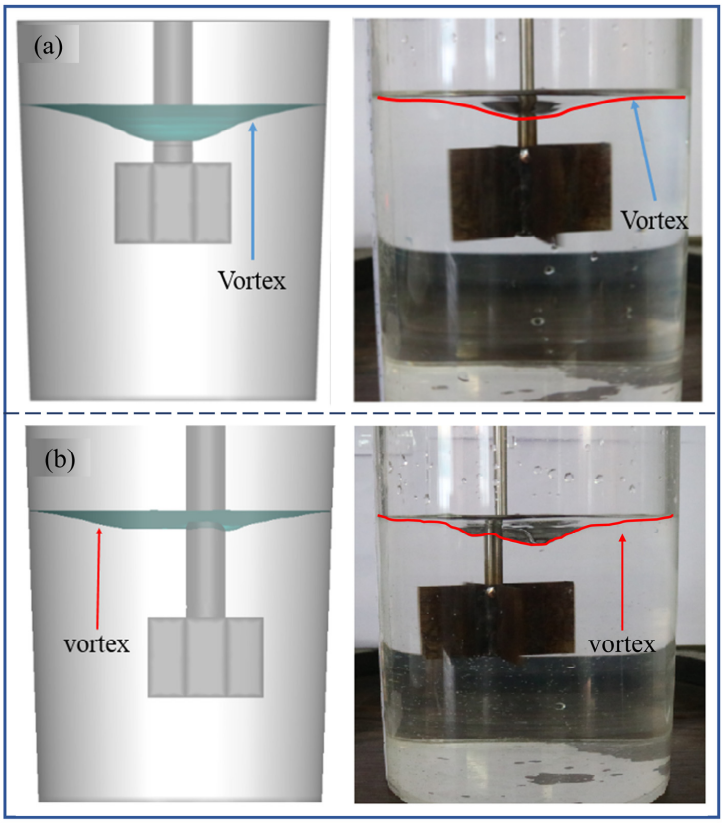

Figure 4. Modeling and water model validation of central and eccentric desulfurization at different depths, with a stirring speed of 120 rpm: (**a**) experimental and simulation comparison of center stirring desulfurization at a depth of 157.5 mm; (**b**) experimental and simulation comparison of eccentric stirring desulfurization at a depth of 217.5 mm.

In the iron desulfurization process, the differences in vortex center offset, as well as vortex shape, depth, and width, between central and eccentric stirring are primarily governed by fluid dynamics principles and the layout characteristics of the stirring paddles. The center of the eccentric mixing vortex deviates from the geometric center of the stirring paddle due to the eccentric arrangement, which disrupts the symmetry of the flow field. This results in an uneven distribution of forces on the liquid, and as the paddle rotates, a biased shear force field is formed. Consequently, the vortex is displaced toward the container wall, and this also leads to the polarization of the stirrer. In contrast, the symmetric flow field of central mixing evenly distributes the thrust of the stirring paddles, ensuring that the center of the vortex aligns with the center of the paddles. The difference in vortex shape is related to the distribution pattern of the flow field: central mixing generates a strong downward flow, resulting in a deep and narrow vortex, while eccentric mixing produces a shallower vortex with a wider coverage at the bottom, due to the more lateral spreading of the fluid. The difference in vortex depth reflects the direction and intensity of the stirring paddle's action on the liquid. The central stirring paddle is more effective at pulling the liquid downward, whereas in eccentric stirring, the uneven distribution of force causes part of the energy to be dissipated in lateral flow, resulting in a shallower vortex with broader coverage. The variations in vortex depth and width result not only from the distribution of the stirring paddle's force but also from the boundary effects and turbulence characteristics. Eccentric stirring exerts a more significant damping effect on the fluid near the vessel wall,

further widening the bottom region of the vortex. The offset of the vortex center, along with differences in shape, depth, and width, results from the symmetry of the flow field, the distribution of stirring dynamics, and the boundary conditions.

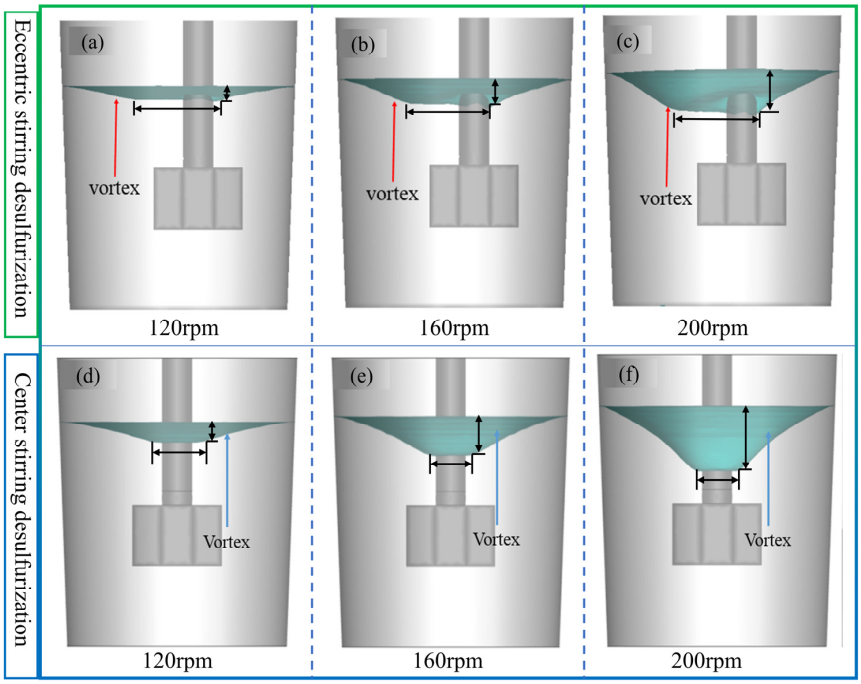

Figure 5. Stirrer immersion depth of 217.5 mm for central and eccentric desulfurization at different rotational speeds. (**a**–**c**) Eccentric stirring desulfurization; (**d**–**f**) Center stirring desulfurization.

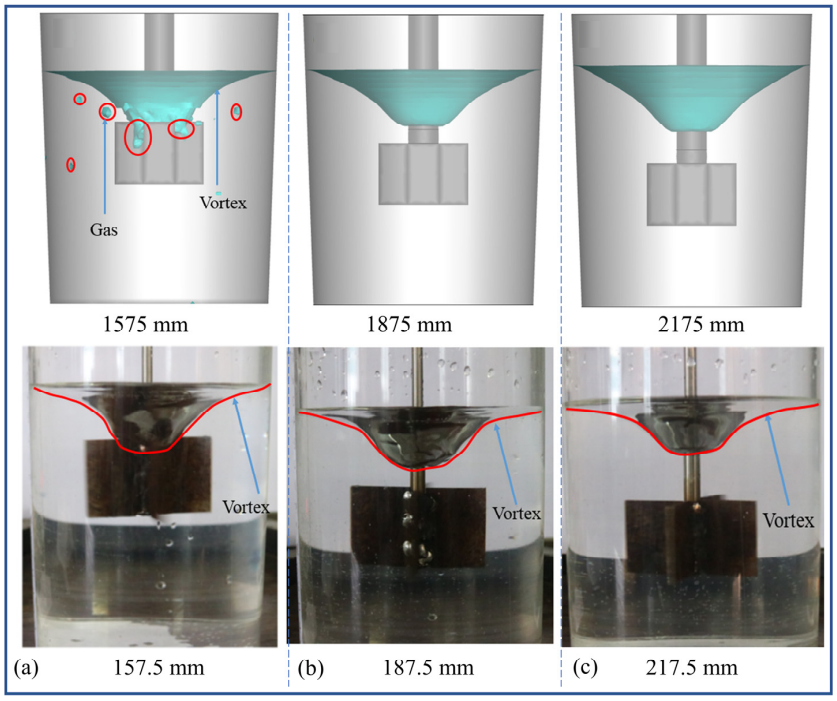

Figure 6. Stirring speed of 200 rpm for central desulfurization modeling at different depths, with water modeling experiments. (**a**) Stirring simulation with the modeled stirring paddle at a depth of 157.5 mm compared to the water model with the stirring paddle at 157.5 mm; (**b**) Stirring simulation with the modeled stirring paddle at a depth of 187.5 mm compared to the water model with the stirring paddle at 187.5 mm; (**c**) Stirring simulation with the modeled stirring paddle at a depth of 217.5 mm compared to the water model with the stirring paddle at 217.5 mm.

4.2. Comparative Study of Central and Eccentric Desulfurization Stirring

To clearly investigate the internal flow-field distribution of hot metal, two cross-sections were selected for flow-field analysis: a horizontal cross-section at Z = 0 and a vertical cross-section at X = 0. Figure 7 presents the velocity field distribution in the horizontal cross-section at Z = 0, with the stirring paddle immersed to a depth of 217.5 mm and operating at a stirring speed of 160 rpm. Figure 7a presents the velocity distribution in the horizontal cross-section of the hot metal under the center stirring mode. The agitator was located at the center of the vessel, and its symmetrical arrangement at 160 rpm resulted in a more uniform flow-field distribution. The velocity vectors exhibit a symmetrical annular structure, indicating that the hot metal is uniformly pushed radially toward the vessel wall and circulates back near the package wall due to fluid resistance. This symmetrical and regular flow pattern not only ensures the uniform distribution of stirring force throughout the vessel but also effectively prevents excessive turbulence in localized areas, thereby providing a stable flow-field environment for the desulfurization process. Central mixing offers significant advantages in flow-field uniformity, which contributes to improved mixing efficiency and the long-term stable operation of the equipment.

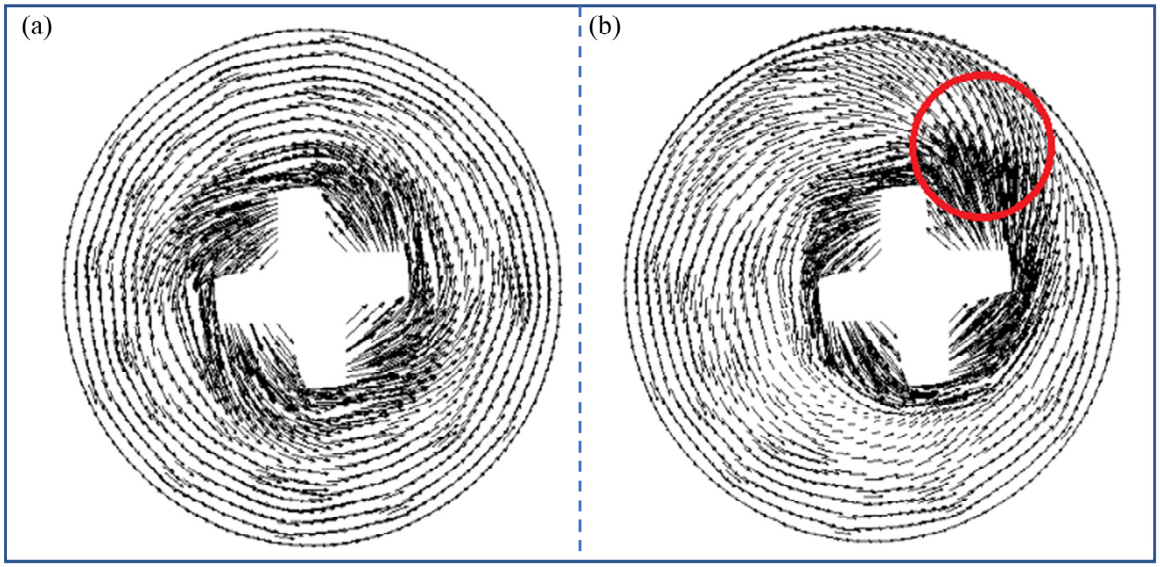

Figure 7. Horizontal cross-section flow-field distribution of eccentric and central desulfurization stirring. (**a**) Horizontal cross-section of molten iron during central desulfurization stirring; (**b**) Horizontal cross-section of molten iron during eccentric desulfurization stirring. The red marked area in (**b**) highlights the uneven distribution of the flow field.

Figure 7b presents the horizontal cross-sectional velocity distribution of ferro-liquid in the eccentric stirring mode. Compared to central stirring, eccentric stirring exhibits significant inhomogeneity in the hot metal flow field due to the asymmetric arrangement of the stirrer. On the side of the stirrer near the package wall (highlighted by the red wireframe), the density of velocity vectors increases substantially, indicating strong fluid disturbance and high turbulence intensity in this region. Conversely, on the side opposite the package wall, the velocity vector distribution is relatively sparse, and the flow intensity is low. Although this flow characteristic sacrifices the overall symmetry of the flow field, the localized strong perturbations promote faster mixing of the desulfurizing agent and hot metal. The asymmetric arrangement of the high turbulence region also allows the stirring action to penetrate deeper into the hot metal, perturbing a larger volume of liquid in a short period of time, which enhances the efficiency of local desulfurization.

To provide a more detailed representation of the velocity distribution, the velocity of the axial section at x = 0 is illustrated using different colors to reflect variations in the fluid flow field, as shown in Figure 8. Below the liquid surface inside the ladle, the regions with relatively strong flow are shown in green, while the blue area below the impeller represents the dead zone. As shown in Figure 8a, when the stirrer was immersed to a depth of 217.5 mm, and the rotational speed was 120 rpm, the velocity field of the hot metal in the center-stirring mode revealed four regular circulating small vortices. These vortices were primarily concentrated around the stirrer, with the hot metal being pushed outward radially by the stirring blades. Upon reaching the package wall, the fluid was split into two streams, flowing upward and downward due to wall resistance. However, such circulating vortices can cause desulfurizer particles in the hot metal to circulate within the region, making it difficult for them to be effectively entrained in the surface and bottom layers of the hot metal, thus limiting the uniform distribution of the desulfurizer. As the stirring speed increased from 120 rpm to 200 rpm, the velocity vector diagram shows that the disorder within the hot metal's internal flow field gradually increased, with axial flow becoming more pronounced. This indicates that the hot metal flow transitions from a regular cycle to a more irregular state. This irregular flow promotes the dispersion of desulfurizer particles and effectively enhances the efficiency of desulfurizer entrainment. As the stirring speed increased, the high-flow velocity region at the bottom of the stirrer expanded, the volume of the hot metal flow dead zone decreased, and the overall stirring efficiency improved significantly. When the stirring speed increased from 120 rpm to 200 rpm, the average velocity of the hot metal increased by approximately 83%, demonstrating the potential for stronger stirring capabilities and improved dead zone distribution.

The velocity field distribution in the eccentric stirring mode, shown in Figure 8b, where the stirrer was immersed to a depth of 217.5 mm, exhibits noticeable asymmetry. On the side of the stirrer near the package wall, the hot metal was strongly squeezed by the stirrer and spread radially outward. Upon reaching the package wall, the flow split into two streams—one flowing upward and the other downward—forming a certain degree of circulating flow. In contrast, on the side opposite the package wall, the flow intensity was weaker, and the velocity vector diagrams show that the hot metal flow rate was lower on this side. This asymmetry resulted in the characteristic flow behavior in the eccentric stirring region: hot metal at the bottom of the stirrer flowed from the side near the package wall to the side opposite the package wall. This improved the flow state of the hot metal in the bottom region and effectively reduced the volume of the flow dead zone. Although the vortex in eccentric stirring was less pronounced than that in the center stirring mode, its flow-field characteristics were more conducive to the diffusion of the desulfurizer at the bottom of the stirrer, thereby enhancing the entrainment efficiency of the desulfurizer in the bottom region. By improving the bottom flow conditions, eccentric mixing can enhance the uniformity of desulfurization to some extent while reducing stagnation in the bottom region.

The difference in velocity field distribution between central and eccentric stirring is primarily reflected in the symmetry of the flow field, vortex structure, the uniformity of concentration distribution, and the flow characteristics of the hot metal at the bottom. Central stirring generates a stable, uniform circulating flow field in the vessel through the symmetrical distribution of stirring forces, characterized by a regular four-vortex structure, which maintains a more stable circulating flow. This approach effectively avoids localized excessive flow or stagnation, reduces the risk of equipment wear, and enhances desulfurization efficiency to some extent. However, the concentrated nature of the vortices may cause the desulfurizer to circulate within specific areas, limiting its dispersion at the surface and bottom of the hot metal. In contrast, eccentric stirring creates a strong localized

disturbance on the side near the package wall through the asymmetric arrangement of the stirrer while pushing the bottom hot metal to flow from one side to the other. This alleviates the problem of flow dead zones at the bottom and facilitates the uniform distribution of the desulfurizing agent in the bottom region. The asymmetry of eccentric stirring also results in an asymmetric flow field, where the ferro-metal movement is intense on the side near the stirrer, while the flow velocity is lower on the side opposite the stirrer, potentially forming a localized stagnation region. This inhomogeneous flow characteristic, while facilitating enhancement in bottom flow and desulfurizer dispersion, also leads to the polarization of the stirrer and erosion of one side of the ladle wall, as observed in the water model, thereby increasing the risk of equipment fatigue. The wear of the stirrer paddles and the erosion of the ladle wall during the actual molten iron stirring desulfurization process must also be considered as critical factors [10]. Additionally, it may lead to the formation of complex turbulent structures at the junction of different flow rates, which affects the uniformity of the desulfurization process. In actual steel smelting processes, central stirring is suitable for smelting modes that require stable and uniform mixing, while eccentric stirring is more appropriate for modes that demand rapid and intensive bottom flow and localized desulfurizer dispersion.

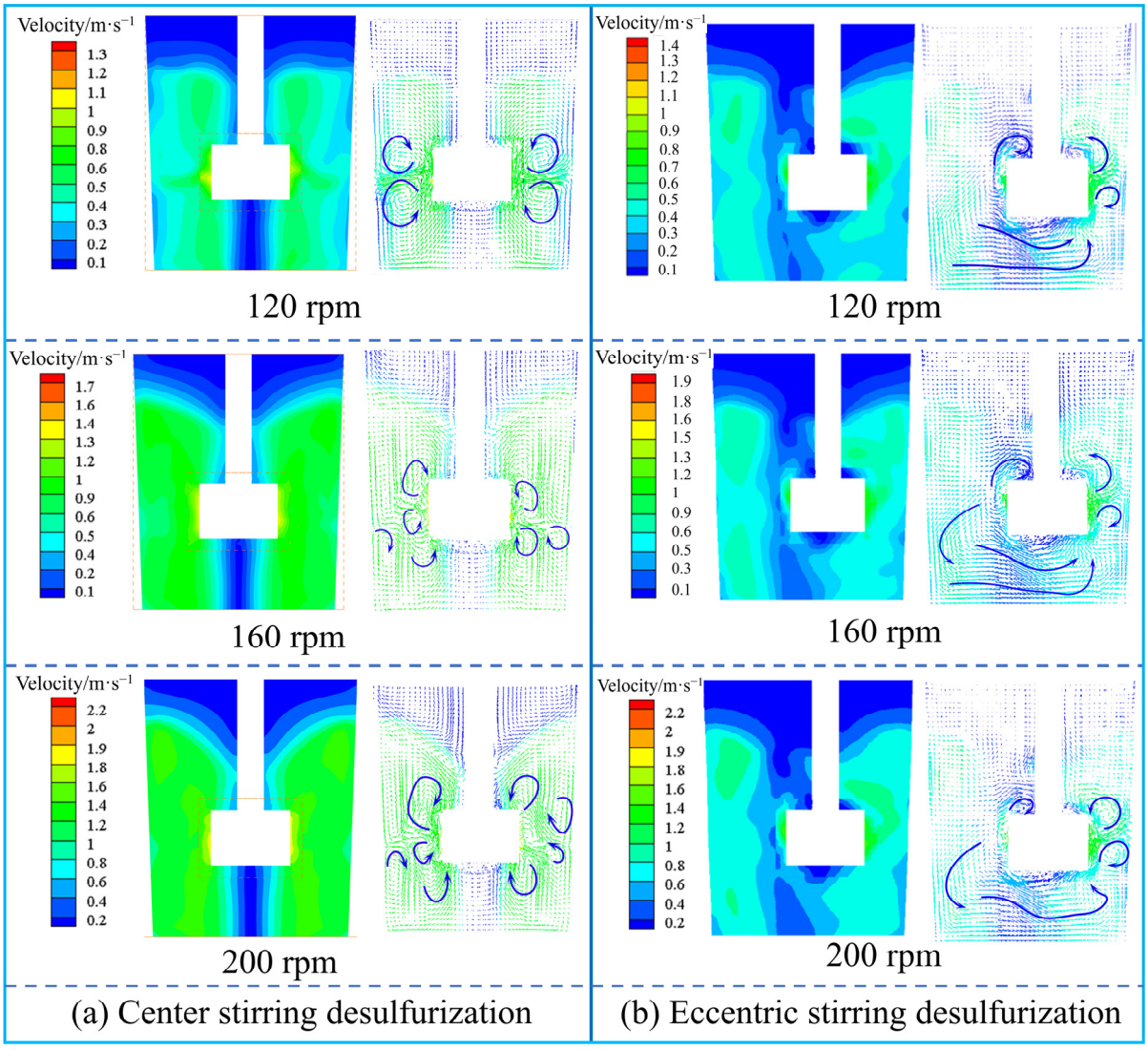

Figure 8. Comparison of flow-field distribution between central and eccentric stirred desulfurization. The blue arrows indicate the flow direction of molten steel in this section.

4.3. Modeling Study of Spherical-Bottom and Flat-Bottom Iron Ladles

Figure 9 illustrates the velocity distribution and velocity vector diagrams for various ladle structures at a stirrer immersion depth of 217.5 mm, with the vertical section taken at x = 0. A comparison of the velocity distributions for the flat-bottom and spherical-bottom iron ladles at different stirring rotational speeds, shown in Figure 9a–c, demonstrates that both the stirring speed and the bottom shape of the ladle significantly influence the flow behavior of the hot metal. At 120 rpm, the flow velocity in the flat-bottom iron ladle is predominantly concentrated near the stirrer, with strong radial flow, which gradually decreases outward along the radial direction. Due to the areas around the stirrer and the stirrer bottom, the iron tends to form tangential flow along the center, resulting in low flow velocities in these regions, which creates a "dead zone". The amount of desulfurization agent entering this area is reduced, thereby lowering the iron desulfurization rate. The comparison revealed that the blue area at the lower part of the stirrer in the spherical-bottom iron ladle is smaller than that in the flat-bottom ladle, indicating that the "dead zone" in the iron flow is reduced. This suggests that the spherical-bottom structure effectively decreases the volume of the "dead zone", thereby improving the mixing of hot metal. At 160 rpm and 200 rpm, as the stirring speed increases, the difference in flow velocity distribution between the two types of ladles becomes more pronounced. The flow velocity in the spherical-bottom ladle varies more smoothly, and the size of the dead zone gradually decreases. In contrast, the flow velocity in the flat-bottom ladle exhibits more fluctuation, with a wider low-velocity zone, particularly near the bottom of the stirrer.

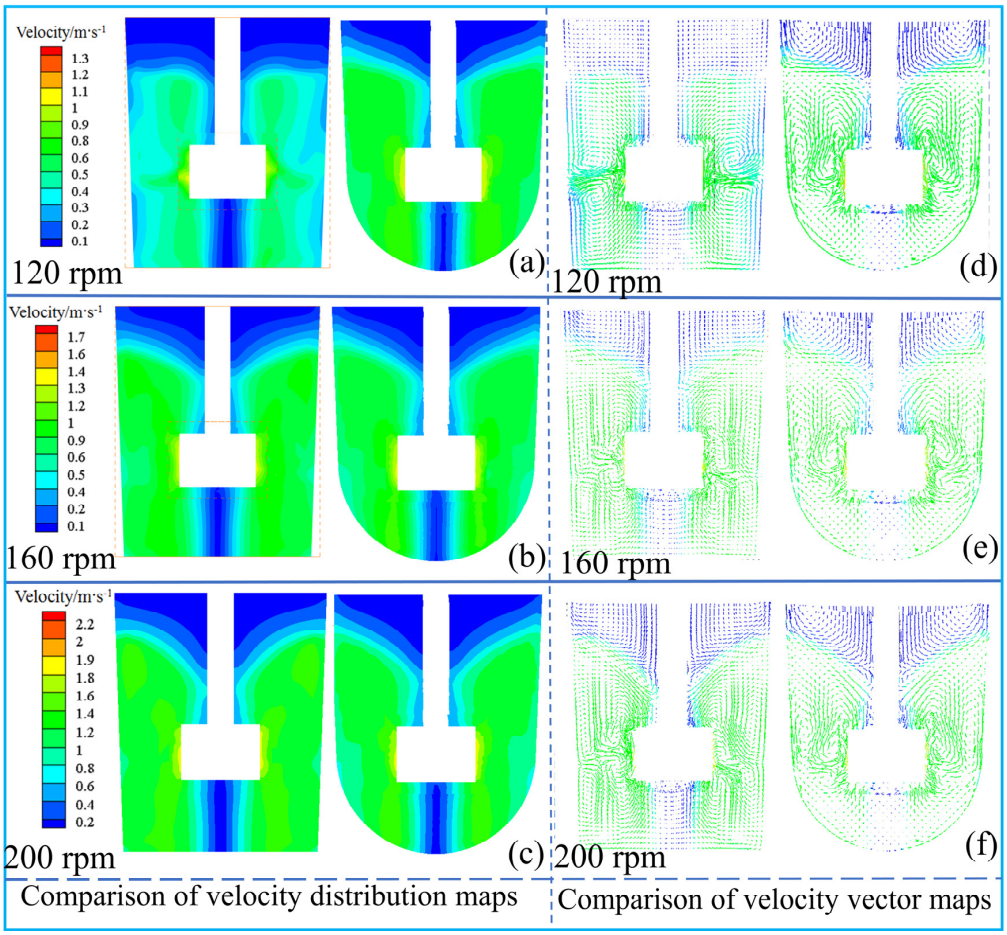

Figure 9. Comparison of velocity distribution and velocity vector diagrams for flat-bottom and spherical-bottom iron ladles. (**a**–**c**) Comparison of velocity distribution maps; (**d**–**f**) Comparison of velocity vector maps.

By comparing the velocity vector diagrams of the flat-bottom and spherical-bottom hot metal ladles at various stirring speeds, as shown in Figure 9, it is observed that the hot metal begins to flow radially from the end of the stirring paddle at the initial velocity. Upon reaching the ladle wall, the flow splits into upward and downward streams. The upward flow, driven by both gravity and the stirring paddle's force, moves upward for a certain distance before gradually descending in a counterclockwise direction, thereby forming a circulation pattern. The maximum velocity is observed at the end of the paddle, with the velocity decreasing radially from this point. This region, located at the paddle's tip, exhibits the most efficient desulfurizer mixing. Additionally, the magnified views of both ladles in Figure 10 highlight differences in the internal flow patterns between the two ladles. In the flat-bottom ladle, a more regular vortex is formed within the hot metal. This regular vortex causes the desulfurization agent to circulate with the hot metal, resulting in a decrease in the relative velocity between the desulfurization agent and the iron, which tends to reduce the kinetics of the desulfurization reaction and negatively impacts the dispersion of the desulfurization agent. In contrast, the spherical-bottom ladle generates an irregular flow pattern, which is more favorable for the dispersion of the desulfurization agent. As shown in Figure 9d–f, there is a distinct flow of the upper hot metal along the ladle wall and the outer side of the stirring center to the bottom of the spherical ladle (indicated by the purplish-red curve traces). This observation suggests that the flow in the spherical-bottom ladle enhances the dispersion of the desulfurization agent. The irregular flow in the spherical-bottom ladle increases the relative velocity between the hot metal and the desulfurization agent, thereby improving the kinetic conditions of the desulfurization reaction.

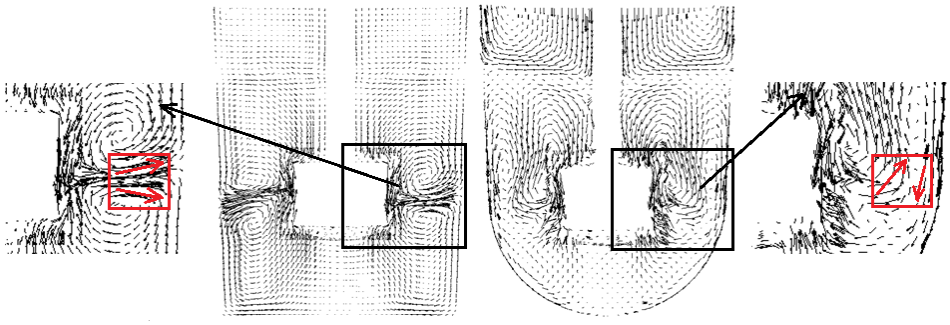

Figure 10. The flow field in a specific area at the rotation speed of 120 rpm. The arrows indicate the flow direction in the marked region.

The hot metal flow velocity is the primary parameter characterizing the hydrodynamic features, directly influencing the involvement and dispersion of the desulfurization agent. To investigate the velocity distribution of hot metal in the ladle, the velocity was measured along two lines within the ladle. One line was parallel to the *X*-axis, 0.1 m from the *X*-axis, which was denoted as Z = −0.1 m, representing the radial velocity distribution, where the negative sign indicates the position below the *X*-axis. The other line was parallel to the *Z*-axis, 0.1 m from the *Z*-axis, which was denoted as Y = 0.1 m, representing the axial velocity distribution. Figure 11 shows the radial velocity distribution at Z = −0.1 m and the axial velocity distribution at Y = 0.1 m for both the flat-bottom and spherical-bottom ladle models, measured at different stirring paddle speeds.

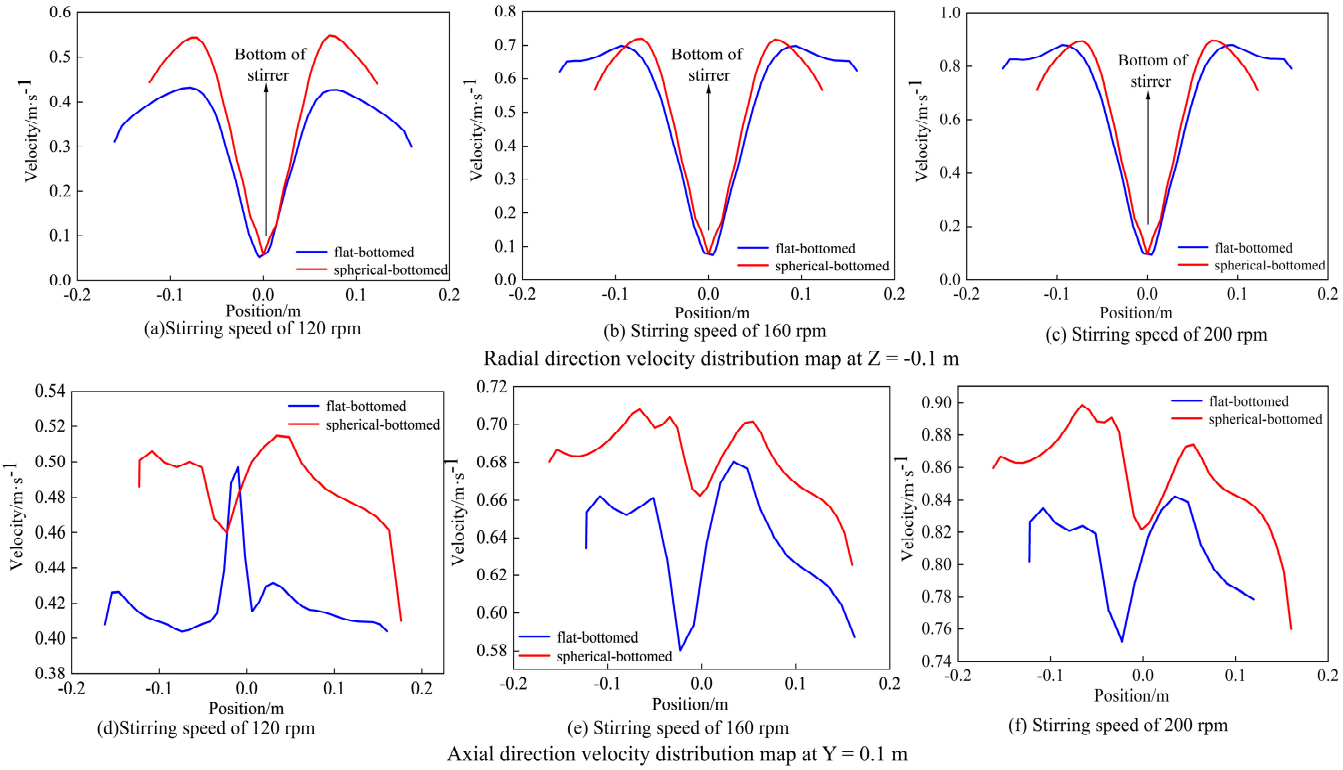

Figure 11. Comparison of velocity distributions.

The radial velocity of hot metal in Figure 11a–c exhibits a roughly V-shaped distribution, which is consistent with the findings of Qiang L. et al. [10]. At the bottom of the stirrer, a tangential flow is formed along the center of rotation, resulting in low flow velocity in this region, which leads to the formation of a "dead zone". Moving outward from the center along the radial direction, the flow velocity of the hot metal gradually increases, reaching its maximum at the end of the paddle. A comparison of the curves for the flat-bottom ladle and the spherical-bottom ladle shows that, at the same position and stirring speed, the flow velocity in the spherical-bottom ladle is higher than in the flat-bottom ladle. This reinforces the conclusion that the spherical-bottom structure enhances the mixing of hot metal and reduces the "dead zone". In the flat-bottom ladle, the radial velocity distribution clearly exhibits a more pronounced "dead zone". Particularly below the agitator, the flow velocity is low, which indicates that the hot metal flows more slowly in the bottom region, leading to reduced desulfurization agent intake in this area and negatively affecting the desulfurization efficiency. The presence of this low-velocity zone impairs the mixing effectiveness. In contrast, the flow velocity of hot metal in a spherical-bottom ladle is significantly higher, especially at the same stirring speed. The spherical-bottom design effectively reduces the volume of dead zones. The curved structure of the spherical bottom enables the hot metal to flow more uniformly along the bottom wall, minimizing stagnation and the formation of low-velocity zones, thereby enhancing flowability. This allows the desulfurization agent particles to be more evenly dispersed within the spherical-bottom ladle, improving mixing efficiency and desulfurization. Furthermore, comparing the curves in Figure 11a–c at the same position, it can be seen that the flow velocity of the hot metal increases as the stirring speed increases. This trend aligns with the principle that higher stirring speeds result in more vigorous iron flow, causing the fluid to expand more rapidly in the radial direction and improving the dispersion of the desulfurization agent.

Figure 11d–f show the axial velocity distribution of hot metal, which exhibits distinct speed peaks and valleys. At the peak of the speed, located at the end of the stirrer paddle,

the flow velocity of the iron is the highest. At the valley of the speed, as shown in Figure 10, the hot metal encounters resistance from the ladle wall, causing it to divide into two streams, one flowing upward and the other downward. In the region between these two streams, the flow velocity of the hot metal is very low, resulting in the "valley" of the velocity distribution. The curve for the spherical-bottom ladle is consistently above the curve for the flat-bottom ladle, indicating that in the axial direction, the flow velocity in the spherical-bottom ladle is greater than that in the flat-bottom ladle.

The velocity accumulation curve represents the percentage of the material's volume within a given velocity range. Figure 12 shows the velocity accumulation graph at different stirring speeds, measured at a stirrer immersion depth of 217.5 mm. As shown in Figure 12a, approximately 66% of the volume of hot metal in the flat-bottom ladle had a velocity in the range of 0.23 m/s to 0.46 m/s, whereas about 76% of the volume in the spherical-bottom ladle fell within the range of 0.24 m/s to 0.61 m/s. As shown in Figure 12b, about 64% of the hot metal in the flat-bottom ladle had a velocity in the range of 0.41 m/s to 0.69 m/s, while approximately 67% of the volume of hot metal in the spherical-bottom ladle was in the range of 0.44 m/s to 0.73 m/s. As shown in Figure 12c, around 65% of the volume of hot metal in the flat-bottom ladle had a velocity between 0.52 m/s and 0.87 m/s, whereas about 65% of the volume in the spherical-bottom ladle had a velocity between 0.54 m/s and 0.9 m/s. It is shown that the volume of high-flow velocity hot metal in the spherical-bottom ladle is greater than that in the flat-bottom ladle at the same stirring speed. A higher percentage of high-flow velocity hot metal indicates that the desulfurization agent can be more uniformly dispersed, facilitating its incorporation into the interior of the hot metal from its surface, thereby enhancing the desulfurization reaction. This, in turn, improves the kinetic conditions for both the hot metal and the desulfurization agent. Furthermore, a comparison of the velocity distributions in the flat-bottom and spherical-bottom ladles at different stirring speeds demonstrates that the percentage of high-flow hot metal increased with higher stirring speeds.

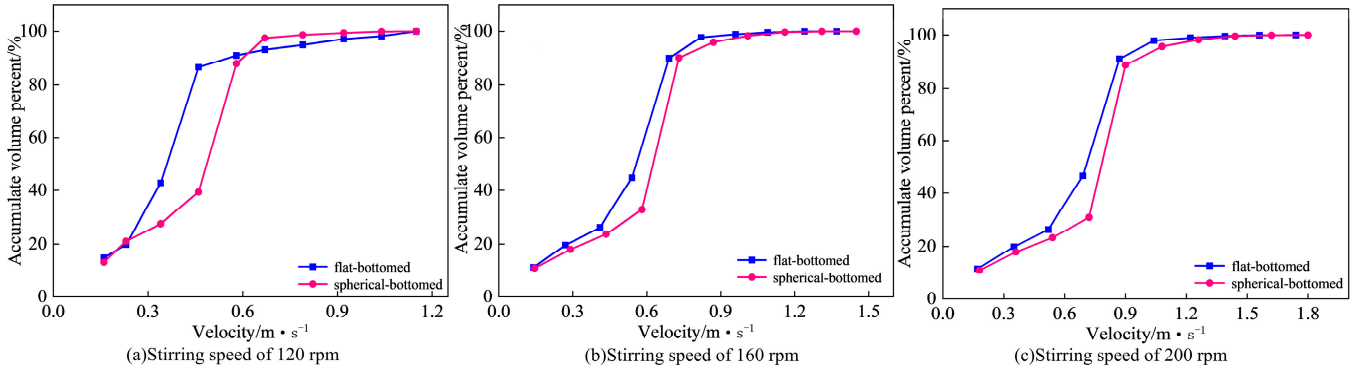

Figure 12. Velocity accumulation curve.

5. Conclusions

In this study, a combination of water model experiments and computational fluid dynamics (CFD) simulations was employed to investigate the impact of ladle geometry on the flow characteristics of hot metal. Conductivity-based mixing experiments demonstrated that the water model experiments closely replicated the desulfurization stirring behavior observed in actual pig iron processes. Numerical models for eccentric and central stirring desulfurization were developed to compare the influence of paddle position on flow dynamics and vortex formation during the desulfurization process. Experimental validation revealed that the simulation results were in strong agreement with the water model findings. The key conclusions derived from this study are as follows:

(1) This study demonstrates that a regular vortex is generated during the central stirring of hot metal, whereas an irregular vortex forms under eccentric stirring conditions, with the vortex axis deviating from the central axis. During the mixing process, the shallow immersion of the stirring paddle often leads to air entrainment, commonly referred to as the "rolled air" phenomenon. Under identical conditions, eccentric stirring desulfurization results in a shallower vortex depth and a larger vortex base area compared to central stirring desulfurization, thereby minimizing the occurrence of air entrainment.

(2) Eccentric stirring creates a high-turbulence region near the mixer and the ladle wall, where the hot metal experiences intensive mixing, while a low-turbulence region forms on the farther side with reduced flow velocity. The flow of hot metal at the ladle bottom moves from one side to the other, effectively reducing the volume of the "dead zone" beneath the mixer. The irregular flow within the high-turbulence region facilitates rapid interaction between the desulfurizing agent and deeper localized layers of hot metal, thereby enhancing desulfurization efficiency.

(3) The uneven distribution of the flow field during eccentric stirring, and the polarization of the stirrer observed in the water model, tend to exacerbate paddle wear and cause the erosion of one side of the ladle wall during actual desulfurization processes. In contrast, the central stirrer creates a stable and uniform circulating flow field within the vessel, which reduces the risk of equipment wear and tear. Therefore, central stirring desulfurization is the optimal choice in actual steelmaking processes, while eccentric stirring desulfurization is only suitable for smelting modes that require a rapid enhancement of bottom flow and quick dispersion of localized desulfurizer.

(4) The spherical-bottom structure of the iron ladle effectively reduces the volume of the iron flow "dead zone" and shortens the mixing time. A comparison of the internal flow fields indicates that, in the spherical-bottom ladle, the upper-layer hot metal flows along the ladle wall and the outer region of the stirring center toward the ladle bottom, which enhances the dispersion of the desulfurizing agent. Additionally, the irregular flow within the spherical-bottom ladle increases the relative velocity between the hot metal and the desulfurizing agent, thereby improving the kinetic conditions of the desulfurization reaction.

(5) In the water model tests, the mixing time for the spherical-bottom ladle was reduced by 22.5% and 20% at different stirring paddle speeds compared to the flat-bottom ladle, which facilitates better dispersion of the desulfurization agents. By comparing the hot metal flow velocities in different regions of the flat-bottom and spherical-bottom ladle models, it can be observed that the flow velocity is higher in the spherical-bottom ladle, which enhances the dispersion of the desulfurizing agent.

Author Contributions: Conceptualization, Q.Y. and L.W.; methodology, Q.Y., L.W. and S.Z.; software, S.Z. and L.W.; validation, L.W. and S.Z.; formal analysis, L.W. and G.W.; investigation, G.W. and L.W.; resources, Q.Y. and S.Y.; data curation, Q.Y.; writing—original draft preparation, L.W. and S.Z.; writing—review and editing, Q.Y. and S.Y.; visualization, S.Z. and G.W.; supervision, Q.Y. and S.Y.; project administration, Q.Y.; funding acquisition, Q.Y. All authors have read and agreed to the published version of the manuscript.

Funding: The work was financially supported by the National Natural Science Foundation of China (52364054).

Data Availability Statement: The raw data supporting the conclusions of this article will be made available by the authors on request.

Acknowledgments: The authors express their gratitude to the National Engineering Research Center for Vacuum Metallurgy at Kunming University of Science and Technology for supporting this work.

Conflicts of Interest: The authors declare no conflicts of interest.

References

1. Wu, S.L.; Wang, L.X.; Lu, Y.A.; Gu, K. Improving the Desulphurization in COREX-3000 Process by the Optimization of Chemical Compositions of Slag. *ISIJ Int.* **2018**, *58*, 2025–2031. [CrossRef]
2. Kapoor, I.; Davis, C.; Li, Z.S. Effect of Residual Elements during the Hot-Working Process of Steel Production: A Critical Review. *Steel Res. Int.* **2024**, *95*, 18. [CrossRef]
3. Hüsken, R.; Cappel, J. Desulphurization strategies in oxygen steelmaking. *MPT Metall. Plant Technol. Int.* **2012**, *35*, 42–51.
4. Li, Q.; Ma, S.W.; Feng, M.X.; Lei, H.; Zou, Z.S. Energy efficiency characterization and optimization of mechanical stirring multiphase dispersion processes: Applied to Kanbara reactors for hot metal desulfurization. *J. Mater. Res. Technol. JMRT* **2023**, *24*, 5642–5659. [CrossRef]
5. Sun, Y.; Chen, W.; Zhang, L.F. Modeling on the Desulfurization of the Molten Steel During RH Process. *Metall. Mater. Trans. B Proc. Metall. Mater. Proc. Sci.* **2024**, *55*, 3950–3960. [CrossRef]
6. Lv, C.; Chen, X.X.; Zhang, H.W.; Zhao, H.L.; Yu, L.H.; Guo, W.M. Simulation study on fluid flow performance of injection stirring composite process in molten iron desulfurization process. *J. Iron Steel Res. Int.* **2023**, *30*, 2403–2415. [CrossRef]
7. Tripathi, P.; Kumar, D.S.; Sah, R.; Sekhar, V.R. An improved lance design for hot metal de-sulphurisation. *Ironmak. Steelmak.* **2017**, *44*, 421–429. [CrossRef]
8. Visuri, V.V.; Vuolio, T.; Haas, T.; Fabritius, T. A Review of Modeling Hot Metal Desulfurization. *Steel Res. Int.* **2020**, *91*, 25. [CrossRef]
9. Su, J.M.; Dou, Z.H.; Zhang, T.A.; Liu, Y. Kinetics of hot metal desulfurization by bottom-blowing magnesium vapor. *J. Iron Steel Res. Int.* **2020**, *27*, 392–401. [CrossRef]
10. Li, Q.; Ma, S.W.; Shen, X.Y.; Li, M.M.; Zou, Z.S. Computational Evaluation of Flow-Induced Abrasion of Blade and Ladle in Kanbara Reactors for Hot Metal Desulfurization. *JOM* **2022**, *74*, 1588–1600. [CrossRef]
11. Nakai, Y.; Sumi, I.; Kikuchi, N.; Tanaka, K.; Miki, Y. Powder Blasting in Hot Metal Desulfurization by Mechanical Stirring Process. *ISIJ Int.* **2017**, *57*, 1029–1036. [CrossRef]
12. Ye, Y. Study of The Properties of Agitatedmixing of Kr Vessel Bywater Model Test. *J. Iron Steel Res.* **1992**, 23–31. (In Chinese) [CrossRef]
13. Luo, A.; Ouyang, D.; Li, M.; Zhu, S.; Jiang, Y.; Wang, H. Research on WG-3Y stirrer for KR desulfurization with water model experiments. *Res. Iron Steel* **2012**, *40*, 31–34. (In Chinese)
14. Ji, J.H.; Li, D.Q.; Du, H.X.; Zhang, S.T.; Yan, S. Effect of Impeller Structure Parameters on Desulfurizer Mixing Behavior in KR Desulfurization Process. *ISIJ Int.* **2023**, *63*, 1334–1342. [CrossRef]
15. Li, X.; Liu, X. Modeling of CaO particles desulfurization for hot metal. *J. Univ. Sci. Technol. Beijing* **2006**, *28*, 237–241. (In Chinese) [CrossRef]
16. Tian, G.; Xu, Q.; Min, T.; Shen, F.; Li, J.; Wang, D.; Xue, Y.; Bao, Y.; Xu, B. Research on Water Modeling in Kr Desulphurization of Hot Metal. In Proceedings of the Metallurgical Research Center 2005 Metallurgical Engineering Science Forum, Beijing, China, 1 April 2005; p. 5. (In Chinese).
17. Xu, A.J.; Zhang, M.L.; Zhang, H.N.; Li, A.D. Simulation of Thermodynamics and Kinetics for KR Desulphurization. *J. Iron Steel Res. Int.* **2011**, *18*, 98–106.
18. Wu, H.; Patterson, G.K. Laser-Doppler measurements of turbulent-flow parameters in a stirred mixer. *Chem. Eng. Sci.* **1989**, *44*, 2207–2221. [CrossRef]
19. Xu, Y.; McGrath, G. CFD predictions of stirred tank flows. *Chem. Eng. Res. Des.* **1996**, *74*, 471–475.
20. Brucato, A.; Ciofalo, M.; Grisafi, F.; Micale, G. Complete Numerical Simulation Of Flow Fields In Baffled Stirred Vessels—The Inner-Outer Approach. In Proceedings of the 8th European Conference on Mixing, Cambridge, UK, 21–23 September 1994; pp. 155–162.
21. Dong, L.; Johansen, S.T.; Engh, T.A. Flow induced by an impeller in an unbaffled tank—II. Numerical modelling. *Chem. Eng. Sci.* **1994**, *49*, 3511–3518. [CrossRef]
22. Tabor, G.; Gosman, A.D.; Issa, R.I. Numerical simulation of the flow in a mixing vessel stirred by a Rushton turbine. In Proceedings of the Fluid Mixing 5 Conference, Bradford, UK, 4–5 July 1996; pp. 25–34.
23. Wang, R.Z.; Jia, S.Y.; He, Z. Numerical Investigation on the Effects of Impeller Structures in Hot Metal Desulfurization Processes by Mechanical Stirring. *Metals* **2022**, *12*, 12. [CrossRef]
24. Ji, J.H.; Du, H.X.; Jiang, Y.; Li, D.Q.; Zhang, S.T. Effect of impellers on particle mixing behaviour in KR desulphurization process. *Ironmak. Steelmak.* **2022**, *49*, 167–177. [CrossRef]
25. Wang, Q.; Jia, S.Y.; Tan, F.G.; Li, G.Q.; Ouyang, D.G.; Zhu, S.H.; Sun, W.; He, Z. Numerical Study on Desulfurization Behavior During Kanbara Reactor Hot Metal Treatment. *Metall. Mater. Trans. B Proc. Metall. Mater. Proc. Sci.* **2021**, *52*, 1085–1094. [CrossRef]

26. Zhao, Y.Y.; Zhang, L.F.; Chen, W.; Cheng, S.S.; Ren, Y. Kinetic modeling on hot metal desulfurization with mechanical stirring. *J. Iron Steel Res. Int.* **2022**, *29*, 719–724. [CrossRef]
27. He, M.L.; Wang, N.; Chen, M.; Chen, M.; Li, C.F. Distribution and motion behavior of desulfurizer particles in hot metal with mechanical stirring. *Powder Technol.* **2020**, *361*, 455–461. [CrossRef]
28. Kato, Y.; Tada, Y.; Urano, K.; Nakaoka, A.; Nagatsu, Y. Differences in Mixing Power Consumption between Dished-Bottom and Flat-Bottom Vessels. *Kag. Kog. Ronbunshu* **2010**, *36*, 25–29. [CrossRef]
29. Chen, W.; Zhao, Y.Y.; Cai, X.Y.; Cheng, S.S.; Zhang, L.F. Water modelling on particle dispersion during KR desulphurization process. *Ironmak. Steelmak.* **2022**, *49*, 707–715. [CrossRef]
30. Kordas, M.; Story, G.; Konopacki, M.; Rakoczy, R. Study of Mixing Time in a Liquid Vessel with Rotating and Reciprocating Agitator. *Ind. Eng. Chem. Res.* **2013**, *52*, 13818–13828. [CrossRef]
31. Mandal, J.; Patil, S.; Madan, M.; Mazumdar, D. Mixing time and correlation for ladles stirred with dual porous plugs. *Metall. Mater. Trans. B Proc. Metall. Mater. Proc. Sci.* **2005**, *36*, 479–487. [CrossRef]
32. Ni, S.Q.; Wang, H.J.; Zhang, J.; Lin, L.; Chu, S.J. A Novel Criterion of Mixing Time in Gas-Stirred Ladle Systems. *Acta Metall. Sin.-Engl. Lett.* **2014**, *27*, 1008–1011. [CrossRef]
33. Jiao, Y.; Zhang, Z.; Gao, F.; Han, J.J.; Wang, J.T. Effects of Particle Suspension on Surface Vortex in Unbaffled Stirred Tanks through DEM-VOF. *Ind. Eng. Chem. Res.* **2024**, *63*, 4662–4677. [CrossRef]
34. Haas, T.; Schubert, C.; Eickhoff, M.; Pfeifer, H. Numerical Modeling of the Ladle Flow by a LES-Based Eulerian-Lagrange Approach: A Systematic Survey. *Metall. Mater. Trans. B Proc. Metall. Mater. Proc. Sci.* **2021**, *52*, 903–921. [CrossRef]
35. Chen, W.; Ren, Y.; Zhang, L.F. Large Eddy Simulation on the Two-Phase Flow in a Water Model of Continuous Casting Strand with Gas Injection. *Steel Res. Int.* **2019**, *90*, 12. [CrossRef]
36. Zhao, Y.Y.; Chen, W.; Cheng, S.S.; Zhang, L.F. Mathematical simulation of hot metal desulfurization during KR process coupled with an unreacted core model. *Int. J. Miner. Metall. Mater.* **2022**, *29*, 758–766. [CrossRef]